



ELSEVIER

Journal of Neurological Sciences 155 (1998) 121–137

JOURNAL OF THE
NEUROLOGICAL
SCIENCES

Two- and three-dimensional computer graphic evaluation of the subacute spinal cord injury

Loren J. Moriarty^a, Bradley S. Duerstock^a, Chandrajit L. Bajaj^b, Kwunlan Lin^b,
Richard B. Borgens^{a,*}

^aCenter for Paralysis Research, Department of Basic Medical Sciences, School of Veterinary Medicine, Purdue University, West Lafayette, IN 47907-1244, USA

^bDepartment of Computer Sciences, Purdue University, West Lafayette, IN 47907, USA

Received 9 December 1996; received in revised form 19 May 1997; accepted 26 June 1997

Abstract

We have evaluated three-week-old compression lesions of the rat spinal cord using two-dimensional and three-dimensional morphometry, reconstruction, and visualization techniques. We offer a new computer assisted method to determine the number and density of macrophages within the spinal lesion using the macrophage specific monoclonal label ED1. We also provide quantitative information on pathological cyst formation and cavitation. This technique does not require: (1) subjective identification of the cell type, (2) human interaction with the data during the phase of quantification, and (3) can be applied to any sampling paradigm based on immunocytochemical labeling. Using novel algorithms based on solutions to 'correspondence' and 'branching' problems inherent in cross-sectional histological data, we provide three-dimensional reconstructions and visualizations of the macrophagic lesions and cysts imbedded within it. Our three-dimensional surface reconstructions can be interrogated to determine volumes and surface areas of structures within the data set. Using these methods we have learned that macrophage numbers approach the maximum density possible for such isodiametric cells (~12 μm diameter) in the central lesion ranging from 4000–7000 cells per mm^2 of lesion. At the time point studied, macrophage numbers would have peaked following the initial insult, and would not be expected to decline for several months. While the density of macrophages is highest in the region of most tissue damage, we show that the central regions of cavitated and cystic spinal parenchyma is not. We discuss how this density of cells may effect the secondary pathological responses of the spinal cord to injury. © 1998 Elsevier Science B.V.

Keywords: Macrophage; Spinal cord injury; Cavitation; 3-D Morphometry; Neurotrauma; Computer graphics

1. Introduction

When the spinal cord is injured, the immediate consequences are not often apparent. A marked destruction of parenchyma occurs with time following the initial insult, and with it, a progressive loss of function. This has led to the term 'secondary injury' or 'delayed' injury (Tator and Fehlings, 1991; Blight, 1992, 1993; Young et al., 1995). There are many hypotheses regarding the underlying

biochemical and physiological processes contributing to secondary injury in the central nervous system (CNS) (Blight, 1992, 1993; Young et al., 1995). These hypotheses are important in that they provide both experimental approaches aimed at preserving behavioral function through intervention with secondary injury, and offer explanations for the efficacy of various clinical treatments.

One view of the cause of secondary injury is curious, perhaps paradoxical, in its suggestion that the inflammatory process produces significantly more soft tissue destruction and loss of function in the CNS than it prevents. One major type of cell mediating this process, professional scavengers of myelomonocytic cell lineage — the macro-

*Center for Paralysis Research, 1244 VCPR, School of Veterinary Medicine, Purdue University, West Lafayette, IN 47907-1244, USA. Tel.: +1 765 4947600; fax: +1 765 4947605.

phage — can be seen in CNS injury as a form of impostor. As cells immigrate into the injury zone, the impressive numbers and density of macrophages create significant ‘bystander damage’. Substantially more demyelination of white matter and cavitation of parenchyma may be produced by these cells than their recruitment prevents during the inflammatory phase of healing (Blight, 1984, 1985, 1992; Perry and Brown, 1992; Perry et al., 1993).

Various other lines of evidence implicate delayed macrophage accumulation, reduced numbers of macrophages, and the state of activation of these cells as playing a critical role in the failure of nerve regeneration observed in mammalian central nervous system trauma (Blight, 1984, 1985; Perry and Brown, 1992; Perry et al., 1993; Lazarov-Spiegler et al., 1996). In spite of the need for accurate determinations of cell number to support these hypotheses or to verify interventions aimed at reducing macrophage accumulations, research of the last decade has emphasized the origins of these cells and not their numbers (Gordon, 1995). Blight (1985) offered the last estimate of macrophage number within a spinal cord lesion using visual identification of macrophages and a line sampling technique. Here we couple immunocytochemical identification of macrophages (ED1 monoclonal label; Damoiseaux et al., 1994) to computer assisted counting and morphometry to define the extent of macrophage invasion, and secondary cavitation of the parenchyma. We evaluate the lesion at 3 weeks post-injury since macrophage numbers would have clearly peaked, and would not be expected to significantly decline over the next 2 months (Blight, 1985). This new means to assess cell number samples between 90 and 100% of the lesion in those histological sections evaluated, and does not require subjective decisions or even human interaction with the data during the phase of quantification. We also use novel algorithms which allow three-dimensional surface reconstructions of the macrophagic lesion. These data confirm elements of our quantitative description of the injury derived from two-dimensional morphometry, and as well validate other formulaic assessments of spinal cord shape and lesion volume previously used in literature. Moreover these reconstructions characterize the extremely complex shape and composition of this soft tissue injury.

2. Methods and materials

2.1. Animals

Fully adult (300–400 g) laboratory rats (Sprague–Dawley) were used in these experiments. Following surgery, they were housed two animals per cage, fed ad libitum, and their health monitored daily. All animals in this study were sacrificed 3 weeks (21 ± 1 days) post-surgery by an overdose of sodium pentobarbital (0.8 ml of 1 g/ml standard injectable) immediately followed by perfusion/fixation with 6% paraformaldehyde, 0.1% glutaraldehyde

in a phosphate buffer. The spinal cords were dissected free and immersion fixed in the above fixative for about 18 h.

2.2. Surgical procedures

Anesthesia was performed using an intraperitoneal injection of 1 ml/100 g body weight of a standardized solution of 10 ml ketamine HCL (100 mg/ml) and 1.1 ml xylazine (100 mg/ml). The spinal cord was exposed by a partial laminectomy (10th to 11th thoracic vertebrae; dura left intact), and the dorsal hemisphere crushed using blunted watchmakers forceps. The incision was closed in layers with 3-0 proline suture, and the skin closed with wound clips. Immediately post-surgery each animal was subcutaneously injected with 3 ml lactated ringers to prevent dehydration, and the animal placed under a heat lamp for about 24 h to reduce post-surgical mortality due to shock.

2.3. Immunocytochemistry

The segment of spinal cord containing the lesion was dehydrated in ascending concentrations of alcohol followed by xylene permitting infiltration and imbedding in Paraplast (paraffin) by conventional methods. The entire spinal cord was sectioned on a rotary microtome at approximately 15 microns, and horizontal longitudinal sections were affixed to microscope slides. Prior to use the slides were dipped in a 0.5% gelatin solution which aids in the adhesion of the sections to the slides during subsequent treatment. Paraffin was partially removed with a 1 h treatment in a 60°C oven, and completely removed after a 1 h immersion in 100% xylene. Sections were rehydrated by immersions in descending grades of alcohol to distilled water by conventional methods.

Hydrated sections affixed to slides were first incubated in a commercial enzyme and tissue non-specific antigen blocker (Endo/Blocker M69 and Tissue Blocker, Biomed) for 5 min, with a 1 min rinse in buffer (Automation Buffer, Biomed). The sections are then exposed to the primary antibody for the macrophage, ED1 [MCA-341, Serotech/Harlan Bioproducts (mouse antirat)] for 10 min, and rinsed with buffer. The secondary biotinylated antibody [rabbit-antimouse (Lab/Probe, Biomed)] was administered for 10 min, rinsed in buffer prior to exposure to the streptavidin peroxidase (10 min), rinsed, and exposed to a commercially prepared diaminobenzidine reagent (Biomed) for 5 min, and counter stained with hematoxylin. Stained sections were rinsed in distilled water and coverslips affixed with a warm glycerol gelatin (Sigma). Two uninjured spinal cords served as controls for non-specific staining.

2.4. Photography and image reproduction

Viewing and conventional photography of spinal cord sections was accomplished with an Olympus Van Ox

universal microscope. Morphometry was performed on digitized images acquired with a JVC TK-1070U color video camera mounted on the microscope (Fig. 1A and B). The acquisition of microscopic images was accomplished with RASTEROPS MEDIAGRABBER 3.2 software captured to a Macintosh Quadra 800 Computer. Working copies of digitized images and data spreadsheets were produced with an HP Laser Jet 5M printer, and final color plates used a Tektronix Phaser 400 dye-sublimation printer.

2.5. Computer assisted morphometry

The method used for the most accurate counting of macrophages within histological sections was based on the determination of an average number of pixels represented by a single macrophage at a standardized magnification (200×). To canvas the lesioned area, one field of view at 200 diameters was chosen within its center and acquired to the computer. Four additional (exactly adjacent) fields of view (rostral, caudal, right and left) were also captured. In this procedure there is no attempt to systematically random sample cells (or parts of cells) within the reference space (the lesion) (Coggeshall and Lekan, 1996). We estimate that in any one spinal cord section, an average of 90% (or more) of the lesion was acquired for cell counting in even the largest injuries. However, in most sections studied, the size of the region of injury was reduced such that 100% of the lesion was acquired, digitized, and managed for morphometry. By using software that can transform assigned color pixel values (color look up tables) to a single color pixel value, the assigned colors (the area of interest) can be measured in pixels (Fig. 1C and D). By sampling every third section (approximately 15 μm), more target area comprised of labeled cells could be evaluated within the histological section than is practical by other sampling/counting techniques. Furthermore, once the visual data is digitized, color transformed for counting, and assigned a file name — the actual counting can be performed using a custom designed script (IPLAB SPECTRUM) that does not require human interaction with the acquisition of this data.

2.6. Macrophage size in pixels

At a standardized magnification of 200 diameters, an average of 14±5 individual macrophage cells (full diameter and isolated from other cells) were chosen per histological section from a series of 12 slides. The mean, S.D. and S.E.M. of these 173 cells in pixels was 18.9, 4.27 and 0.3 respectively. The actual unit area of the pixel in micrometers at this same magnification was determined by capturing an index score of a haemocytometer to the computer. We also made measurements of the diameters of 61 similarly isolated macrophages, using an ocular micrometer for comparison of the means.

2.7. Algorithms for three-dimensional surface reconstruction and quantification

For 3-D reconstruction, the spinal cord segment containing the lesion was acquired to the computer at low magnification (20 diameters). All serial histological sections comprising a spinal cord were used for this purpose. During the digitization process, registration was accomplished by superimposing each successive image onto a tracing of the prior histological section made on the computer screen with a dry erase marker. The boundary of the cord, and other fiducial points or objects (such as cysts and irregularities of the lesion) served to aid in serial registration.

The algorithms used in this study construct planar contours of cord, lesion, and cysts as images via a process of segmentation. The constructed planar contours are polygons. The task is to construct surface meshes which interpolate the contours on two adjacent histological sections. Each section contains zero or more non-intersecting polygons which may be nested. The 3-D surface construction from planar contours requires a solution to correspondence, tiling, and branching problems.

The correspondence problem involves finding the correct connections between the contours of adjacent histological sections. Tiling refers to the use of boundaries to triangulate the strip lying between contours of adjacent sections into triangles. A branching problem occurs when a contour in one section may correspond to more than one contour in an adjacent section. The possibility of branching significantly complicates the task of tiling.

We approach the solution to all of these problems simultaneously (Bajaj et al., 1996a). This is accomplished by imposing a set of three mathematical constraints on the reconstructed surface and then deriving precise correspondence and tiling rules from these constraints. The constraints ensure that the regions tiled by these rules obey physical constructs and have a natural appearance.

Once a surface (wire frame or tiled mesh) is constructed, quantitative interrogation of the reconstruction to provide precise surface areas and volumes can be accomplished. The surface area of the 3-D image is simply the sum of all triangles. If the tiling process does not develop any untiled region, the reconstructed shape is a prismatoid which is a triangular tiled region between two parallel contours. If the reconstructed shape is not a prismatoid, it can be reduced into prismatoids (Bajaj et al., 1996b). A prismatoid is a polyhedron which consists of two planar contours in parallel planes and lateral triangles. The three vertices of each lateral triangle must be the vertices of both planar contours. The volume of a prismatoid is calculated as $V = h/6 (B_1 + 4M + B_2)$ where B_1 is the area of the lower base, B_2 is the area of the upper base, M is the area of the midsection joining the bases and h is the separation between contours. With n parallel slices of contours equally spread, the composite volume computation results in: $V_1 = \frac{h}{6} (B_1 + 4 \sum_{i=1}^{n-1} M_i + 2 \sum_{i=2}^{n-1} B_i + B_n)$.

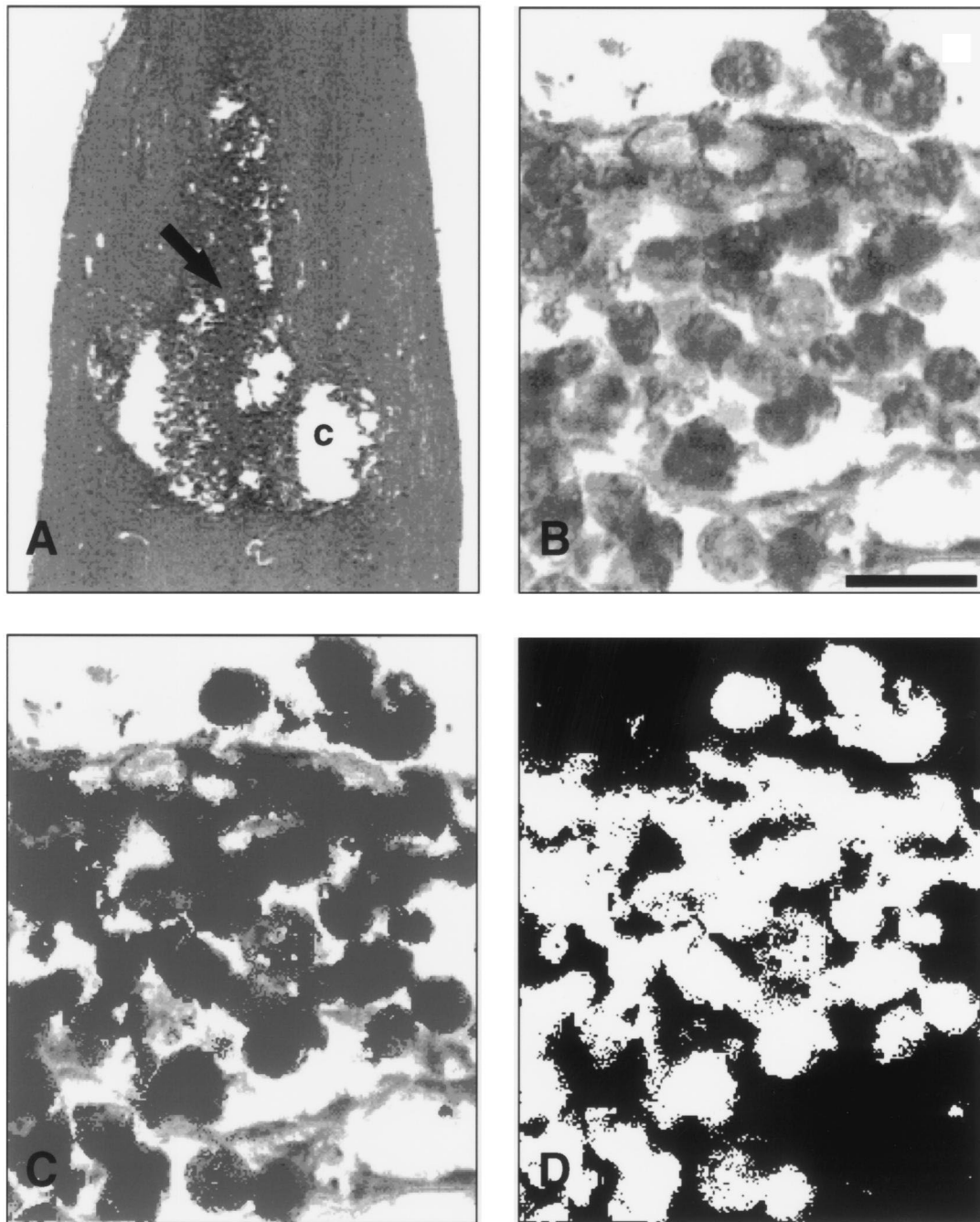


Fig. 1. ED1 Immunocytochemistry: Two-dimensional morphometry. (A) Longitudinal horizontal section of a rat spinal cord, oriented rostral to the top and caudal towards the bottom. The section is 2.5 mm at its widest. This digitized image is as it appears on the video monitor following capture from the histological section (see methods). The dark purple/brown staining (arrow) is the region of labeled macrophages delineating the centrally located spinal cord lesion. The spinal cord is counter-stained with hematoxylin. Such compression lesions at 3 weeks were usually cystic (C). (B) A similarly digitized high magnification view of individual ED1 labeled macrophages within the injury site of the spinal cord shown in A. Note the vesiculated appearance of some of the labeled phagocytes and the blue background staining of strands of parenchyma. Scale bar = 20 μm . (C) The identical image shown in B. The pixel values showing the overall range of brown staining (labeled macrophages and portions of macrophages) has been converted to a single pixel value (green) in preparation for binarization and computer assisted counting. Note the exclusion of the blue stained parenchyma shown in B. (D) The identical image shown in B and C. To facilitate counting, the image is binarized where the pixel value of 1 (white) is ascribed to the macrophages and all other color values = 0 (black). The computer assisted program of counting then derives the unit area in white pixels. At any given magnification, the unit area in pixels is further converted to the unit area in micrometers (see Section 2).

Table 1

Type of measurement	Animal number	Number of macrophages measured	Mean cell diameter (pixels)	Mean cell diameter \pm S.E.M. (μm)	Mann–Whitney <i>U</i> (two-tailed, unpaired)
Visual	8	61	N/A	12.77 \pm 0.50	<i>P</i> = 0.72
Computer	12	173	18.87 ^a	12.47 \pm 0.21	

^a 1 μm = 1.51 pixels at 200 \times .

2.8. Statistical evaluation

Comparison of data sets used Wilcoxon, Mann–Whitney *U*, and paired two-tailed student's *t* tests of significance. Computations were performed using INSTAT software.

3. Results

3.1. Verification: macrophage cell diameter and cell counting

As described previously, the mean cell diameter in pixels of 173 individually measured cells was 18.9 \pm 0.3, while the mean diameter by actual measurement was 12.5 \pm 2.7 μm . We compared this average diameter with other histological examples of macrophages taken from the literature (11–21 μm ; Blight, 1985, 1992), and we made micrometer measurements of the diameter of 61 individual and isolated macrophages as an additional check. In brief, our computer derived estimate of the macrophage cell diameter was very similar to the direct measurements and not significantly different (Table 1).

The accuracy of our computer assisted computation of macrophage number based on pixel values/macrophage was also verified by comparing computer assisted counts of macrophages within ten different fields of view at our standard magnification with actual cell counts of these same fields of view made by a naive investigator. These numbers were also close, and were statistically similar (Table 2).

3.2. Macrophages of the subacute lesion

In every injured spinal cord, macrophages were the dominant cell type occupying the site of damage. Given the dorsal approach to the spinal cord during the laminectomy procedure, followed by compression of the dorsal spinal cord, one would reasonably expect the lesion

severity to be most profound here in all eight spinal cords. This was true, and best exemplified by two spinal cords in which the tissue damage was completely confined to the dorsal half. Fig. 2 shows the typical dorsal to ventral extent of lesioned parenchyma in two spinal cords where a variable amount of ventral grey and white matter destruction was evident. We measured the rostral to caudal extent of compromised spinal cord in all of the samples (measuring this in every third section beginning at the most dorsal). At T11 (the approximate lesion site in most cords) the length of the spinal cord segment is approximately 4.5 mm, at T12, 4.3 mm, and at T10, 4.6 mm (see Waibl, 1973). The average measured rostral/caudal extent of the lesion for all 8 animals was 3.8 \pm 0.7 mm (Table 3). Thus the longitudinal extent of the injury was somewhat less than one vertebral segment.

As discussed, labeled macrophages were of typical size (between 10 and 16 μm diameter), vesiculated with numerous inclusions, and positive for surface antigens derived from rat macrophage (ED1) (Fig. 1B, Fig. 3A and B). We did not observe artifactual staining or labeling in control sections of two uninjured cords.

3.3. Lesion boundary

The boundary of the injured region of spinal cord was well defined due to large accumulations of labeled macrophages separating relatively undamaged parenchyma (visualized by the counter stain) from macrophage filled and usually cystic spinal cord parenchyma (Fig. 1A, Fig. 2). The integrity of adjacent 'intact' spinal cord tissue showed well defined cell borders, homogeneous staining with hematoxylin, and was relatively free of phagocytes. These regions sometimes possessed variable amounts of cavitation, however. The boundary of the lesion and large cysts was circumscribed on the digitized image using a laboratory designated tracing program. This procedure was carried out on every digitized histological section of each cord as a first step in creating 3-D surface reconstructions.

Table 2

Type of measurement	Animal number	Fields of view counted	Mean macrophage count \pm S.E.M.	Wilcoxon (two-tailed, paired)
Visual	7	10	55.6 \pm 16.1	<i>P</i> = 0.56
Computer	7	10	59.5 \pm 21.3	

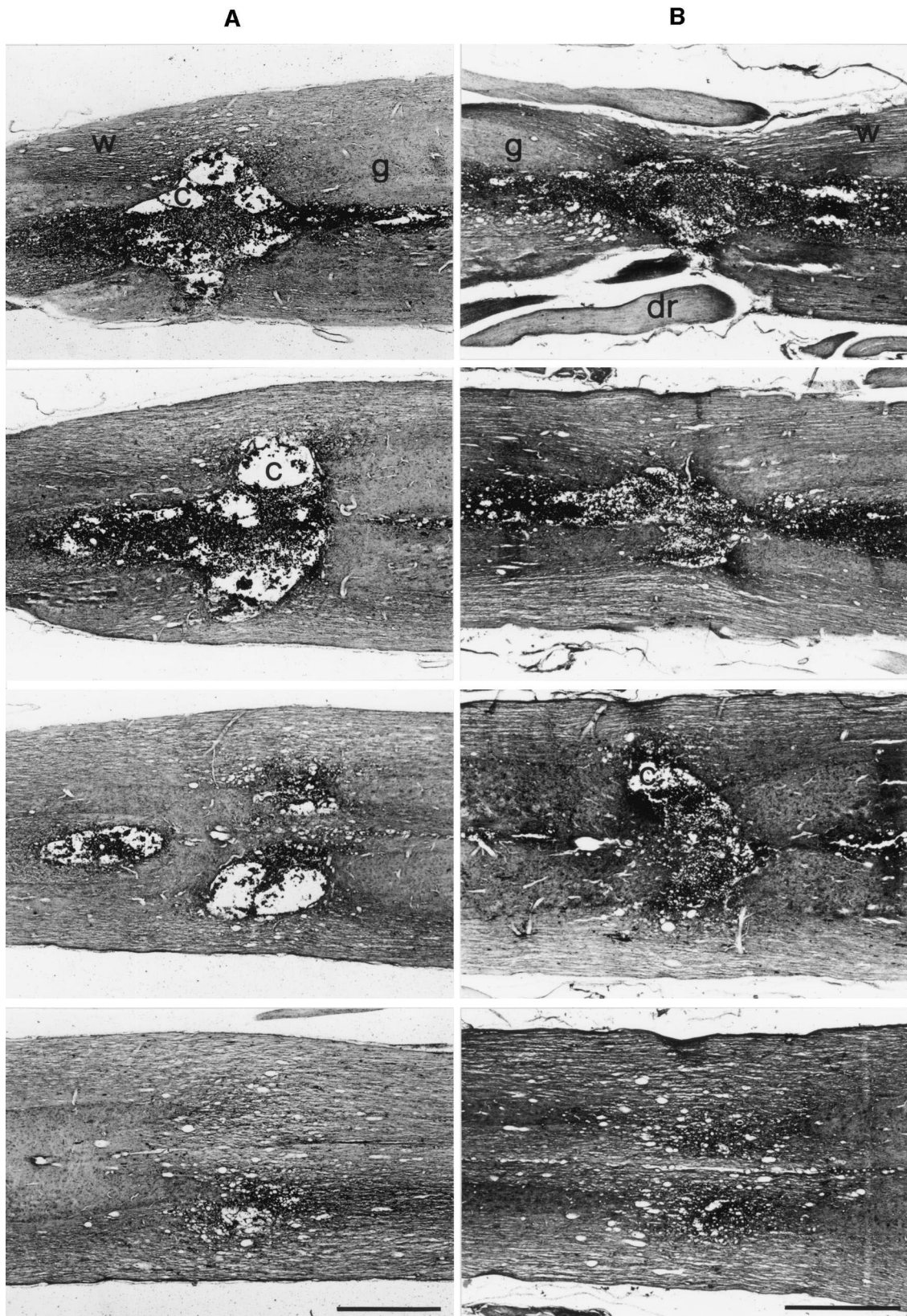


Fig. 2. Examples of spinal cord injuries comprising the data set. The four images in column A are individual sections of the same spinal cord showing the progression of a compression lesion from dorsal (top of page) to ventral (bottom of page), and similarly in B. Both cords are oriented rostral to the left and caudal to the right. One section of the spinal cord in column A was shown digitized in Fig. 1. Note in both spinal cords the dark regions of macrophage staining in both white and grey matter is usually localized in and around cysts at the site of actual compression of the spinal cord. Note that the cord in column A is more cystic than the one in B. Note in both spinal cords, accumulations of macrophages are extensive in the dorsal white matter, and less extensive in both grey and white matter in more ventral regions of the spinal cord. This is probably due to the dorsal focus of compression (see Section 2). Scale bars in the bottom photomicrographs for column A and B=1 mm, (dr, dorsal root; w, white matter; g, grey matter and c, cysts.)

Table 3
2-D Morphometry of cysts and cavities

Rat no.	Cysts mean diameter (mm)		Rostral cysts mean area (mm ²)		Caudal cysts mean area (mm ²)		Microcavities mean diameter (μm)		Lesion length (mm)
	<i>n</i> ^a		<i>n</i> ^b		<i>n</i> ^b		<i>n</i> ^a		
1	14	0.31	3	0.91	3	0.77	10	15.6	4.2
2	7	0.10	2	0.17	2	0.28	10	15.6	4.0
3	8	0.11	2	0.21	2	0.09	10	14.9	3.5
4	10	0.13	2	0.17	2	0.12	16	11.9	5.3
5	10	0.26	2	0.61	2	0.27	13	14.5	3.2
6	6	0.10	2	0.13	2	0.11	8	14.0	3.0
7	7	0.15	3	0.17	3	0.09	14	16.8	3.7
8	9	0.13	2	0.15	2	0.24	10	18.3	3.2
<i>n</i>	71		18		18		91		24
Population mean		0.18		0.14		0.11		15.0	3.8
Population S.E.M.		0.02		0.03		0.02		0.5	0.3

n, The number of cysts measured in each animal's spinal cord.

^a The diameter for each cyst was obtained by averaging the major and minor axis.

^b The area for each cyst was determined by Pixel transformation (as for macrophages) using IPLAB SPECTRUM (see methods).

3.4. Macrophage counts

At 3 weeks post-injury, macrophage numbers were quite variable between spinal cords as well as within individual histological sections of the same spinal cord. Individual sections contained numbers of macrophages ranging from a few hundred cells to over 2000, with means ranging from approximately 500 to 1500 cells per section. These counts were confined to the lesioned region of spinal cord and do not represent the numbers of macrophages that could be found at greater distances from the focus of injury (such as within degenerating white matter tracts). Additionally, we emphasize these numbers are conservative ones, or under-represent the actual numbers of cells in even the focal site of damage since in some sections less than 100% of the lesioned area was sampled by our technique. Fig. 4 provides examples of macrophage counts and the unit area they occupy for three individual spinal cords (A) and a summary of all eight cords studied (Fig. 4B). In spite of the large and expected variation in cell numbers, the greatest numbers of macrophage cells were found in the dorsal half of the spinal cord — that region associated with the greatest damage produced by dorsal compression of the cord (see methods). This is more evident when the macrophage counts are normalized by peak values (Fig. 5), showing increasing cell counts peaking near the central — but still dorsal — region of the spinal cord, and decreasing sharply in ventral regions. The peak densities of macrophages represent a very significant fraction of spinal cord in regions where substantial numbers of these cells accumulate. The unit area occupied by macrophages in the lesioned segment ranged from 0.1 to 0.2 mm² within dorsal spinal cord segments of approximately 0.7 mm².

3.5. Cystic regions within the injury zone

Though we made no comprehensive effort to quantitate

the various fluid filled cavities that form in response to spinal cord compression, we did measure the diameters of two separate types of cavities that were common in all eight cords studied. Large cysts that were centrally located within the region of injury and appeared to be in continuity with the swollen central canal (Fig. 1A, Fig. 2 column A, Fig. 6A, B) were on the order of 0.2 mm in diameter (*n*=71) (Table 3). The largest cavities in central regions of grey matter were on the order of 25–30% of diameter of the uninjured spinal cord. In all spinal cords but two, these cavities were larger rostral to the injury than caudal. In spite of this trend, we detected no statistical difference relative to the rostral/caudal side of the injury in which the largest cysts occurred (*P*=0.06, paired Student's *t*) (Table 3).

Another commonly observed form of cystic cavitation in all animals was so-called 'microcavitation.' These cavities were not necessarily associated with the focal area of damage. Regions of microcavitation were sometimes extensive in white matter tracts undergoing Wallerian degeneration (Fig. 6C and D). For example long tracts such as the ascending dorsal columns and lateral white matter tracts were intact on the caudal side of the injury, but degenerate on the rostral side — sometimes for the entire length of the histological segment examined. Phagocytosis of these distal segments produced expanses of cystic white matter where the average diameter of the individual cysts were curiously about one macrophage cell diameter (15±5 μm; *n*=90; Table 3). It is likely the most active phagocytosis in these areas occurred prior to our sample time of 3 weeks as cavitated regions of white matter did not contain the dense accumulation of macrophages that were observed at the focal region of spinal cord damage. In three of the eight spinal cords containing degenerate white matter tracts, these regions were nearly free of ED1 labeled cells.

Computer assisted two-dimensional counting allowed an

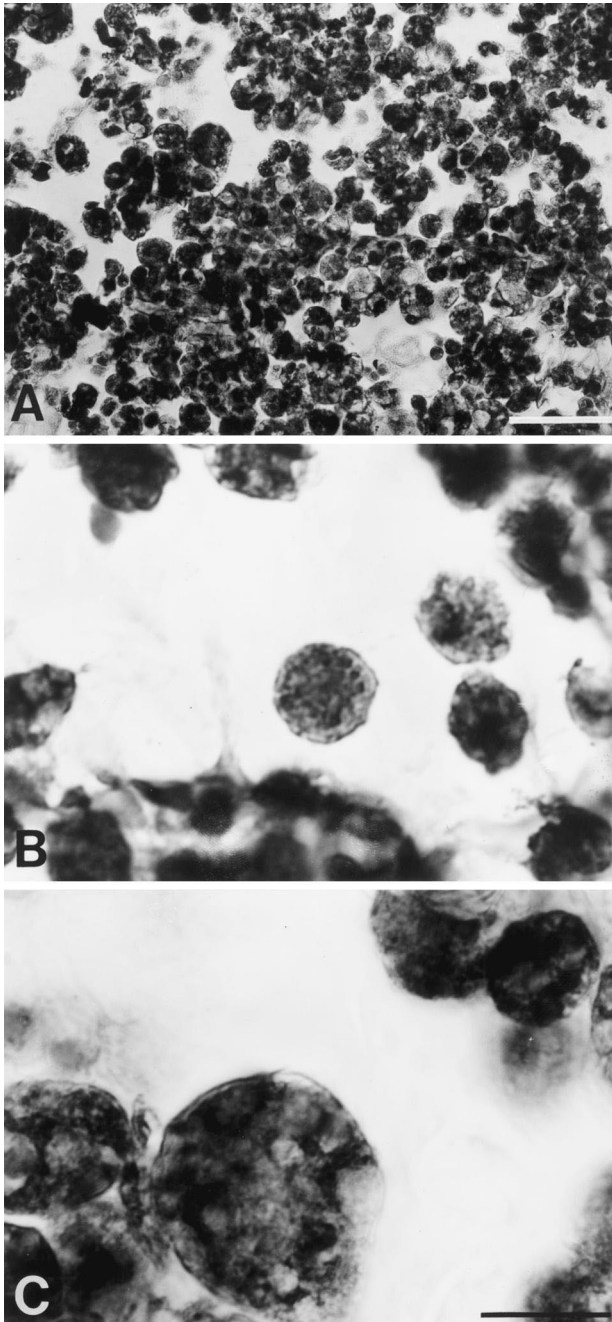


Fig. 3. Photomicrographs of ED1 labeled macrophages. (A) Accumulation of ED1 labeled phagocytes within a cystic area of spinal cord. As shown in the previous digitized image (Fig. 1B), these cells are roughly spherical, approximately 15 μm in diameter, and vesiculated. Even in relatively dense areas of cell accumulation, individual cell profiles can be seen in 15 μm thick histological sections. The scale bar in A = 100 μm . (B) High magnification view of labeled macrophages for comparison to C, which shows ED1 positive giant macrophage cells. The scale bar shown in C = 30 μm for photomicrographs C and B. Note the giant cells in C are approximately 3–4-fold larger than the normal macrophage, and possessed multiple nuclei (data not shown).

approximation of the total unit area of cysts at the lesion site, since large cavities within the region of damage were color transformed and their unit area measured in pixels in

the same manner as performed with stained macrophage cells (see Section 2). The total unit area of these cysts ranged from about 0.025 to 0.1 mm^2 within any one histological section of a lesioned cord. Fig. 7 shows three representative examples of such measured cysts (A) and a summary for all eight spinal cords studied (B). Note that in contrast to the character of macrophage accumulations, the regions of spinal cord containing the greatest density of cysts does not correlate with the region of greatest experimental compression.

3.6. Defining the area of the lesion

If we are to evaluate the peak accumulations of macrophages relative to the size of the histological lesion at 3 weeks post-injury, we must first define what the 'lesion' is. In one scheme, we can define the lesion as that region of damaged parenchyma bounding macrophage accumulation that as well contains fluid filled cysts. This would be the more routine way an examiner would usually circumscribe the boundary of a 'lesioned area' on any one histological section. It would be fair to include cysts within this region since many contain aggregations of phagocytic cells which may be ingesting — or at least obscuring — damaged parenchyma [see also such 'floating' macrophage accumulations in Blight (1992)]. However, there are usually islands of relatively intact parenchyma, well defined by background staining within such an area of injury. In another scheme, one might consider this relatively intact parenchyma (free of macrophages) as uninjured, and define the lesion as the area composed of macrophages and cavitated parenchyma, but not including internal zones — or islands — of relatively intact grey and white matter. Fig. 8A shows a summary graph of the area of damaged, macrophage infested, and cystic spinal cord parenchyma. Fig. 8B shows a similar graph in which undamaged parenchyma contained within this zone has been deleted from the calculation of unit area. A simple inspection of the ordinates demonstrates this difference in unit area of lesion to be substantial.

3.7. Macrophages per unit area of lesion at 3 weeks post-injury

Fig. 8C shows total counts of macrophages per unit area of lesion. In Fig. 8D the data represents macrophages within lesions in which islands of relatively undamaged parenchyma are not included. Note that accumulations within the damaged dorsal hemisphere of the spinal cord range from 4000–7000 cells per mm^2 of lesion using the latter definition of the lesion. The more routine way of defining the lesion (which does not take into consideration zones of apparently healthy parenchyma) shows the macrophage accumulations to be less than half of this amount (Fig. 8C).

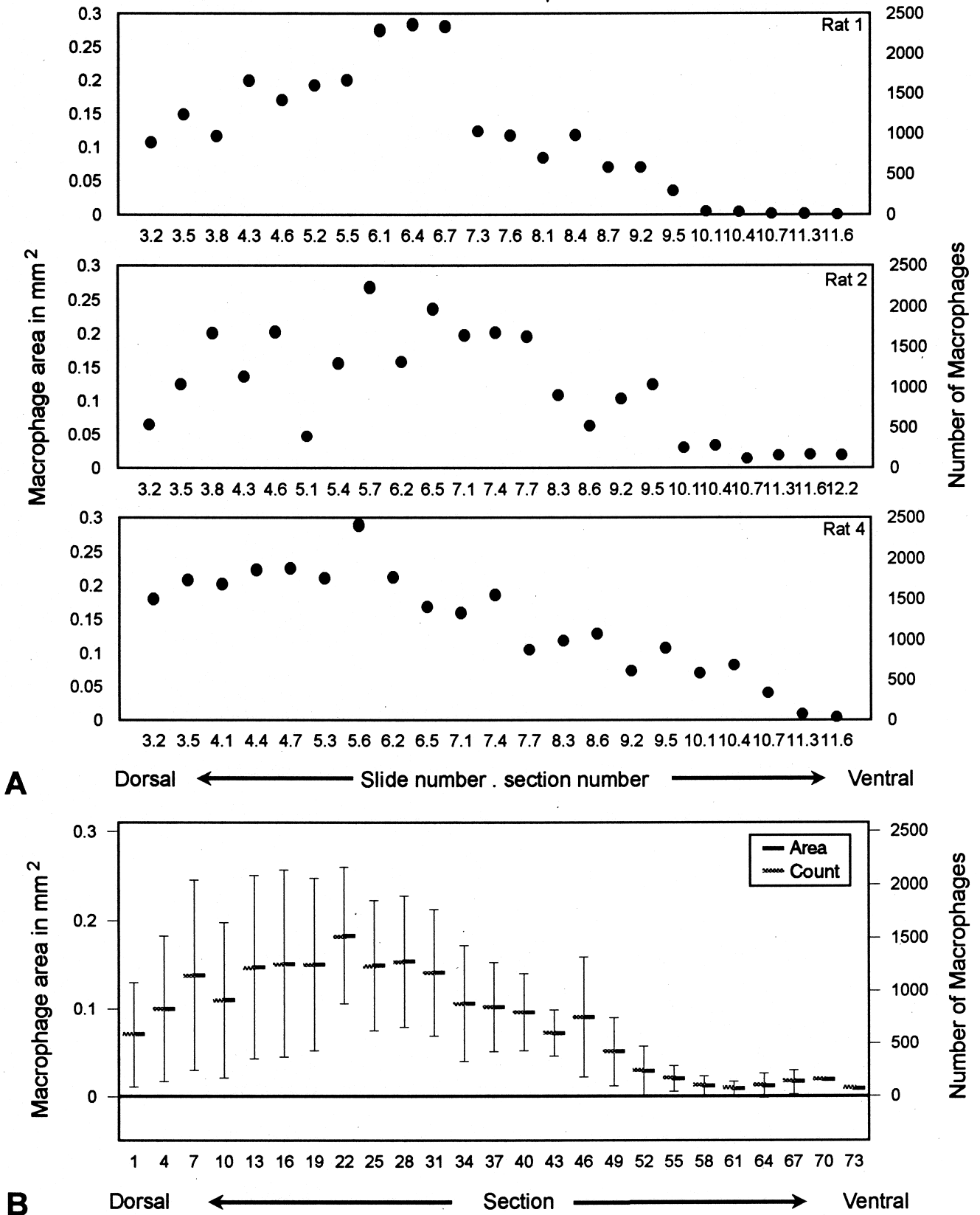


Fig. 4. Macrophage unit area and number by histological section. (A) shows examples of area and number plots for rats 1, 2, and 4. (B) shows the means and S.D.'s of all 8 rats.

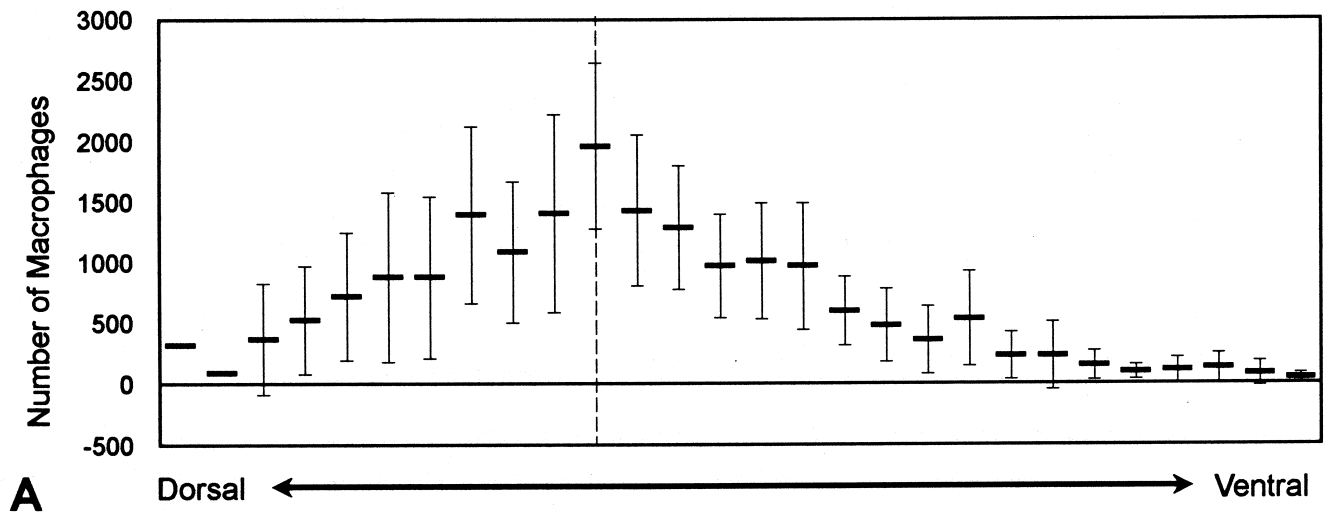


Fig. 5. Macrophage counts normalized by peak values. The hatched line represents the section containing the maximum number of macrophages for each spinal cord. Means and S.D.'s for the sections dorsal and ventral are distributed on either side of this peak.

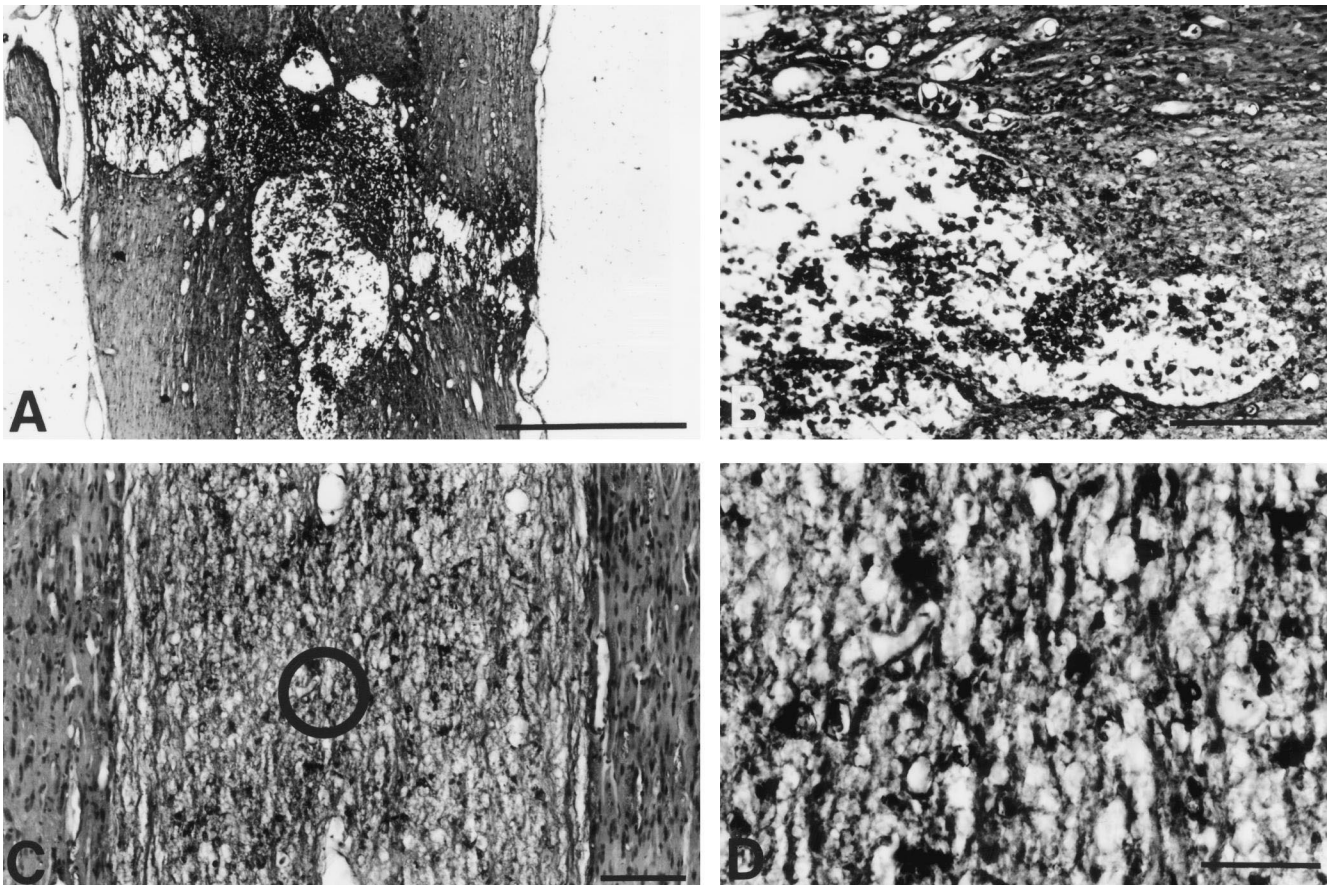


Fig. 6. Cyst and microcavities in damaged spinal cord parenchyma. A typical zone of compression injury is shown in A, containing numerous large and small cysts. It is likely that the large cysts located within the central cord are part of, or connected to, the central canal. The numerous smaller cysts in this locale (B) may or may not be connected as a cisternal system containing CSF. In regions far from the area of compression, white matter tracts undergoing Wallerian degeneration are always extensively cavitated (C and D). These small cavities are on the order of one cell diameter (10–15 μm). The defining of cysts and microcavities was not arbitrary in this report, but reflects a difference in the location, size, and significantly different range of diameters in the two groups of cavities quantitated by 2-D morphometry (Table 3). Scale bars: A=1 mm, B=250 μm , C=100 μm and D=50 μm .

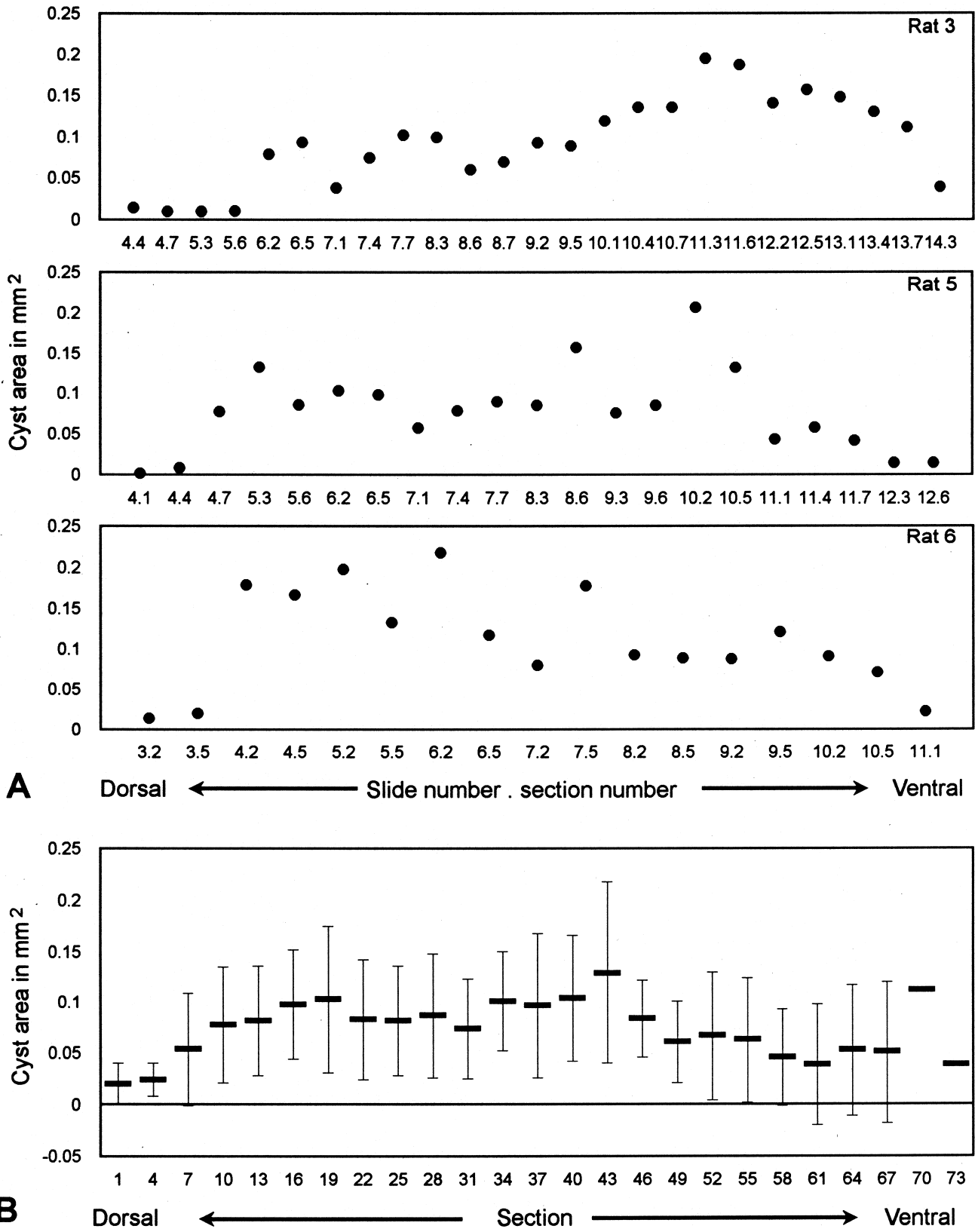


Fig. 7. Cyst area by histological section. (A) shows examples of area plots for rats 3, 5 and 6. (B) shows the means and S.D.'s of all 8 rats.

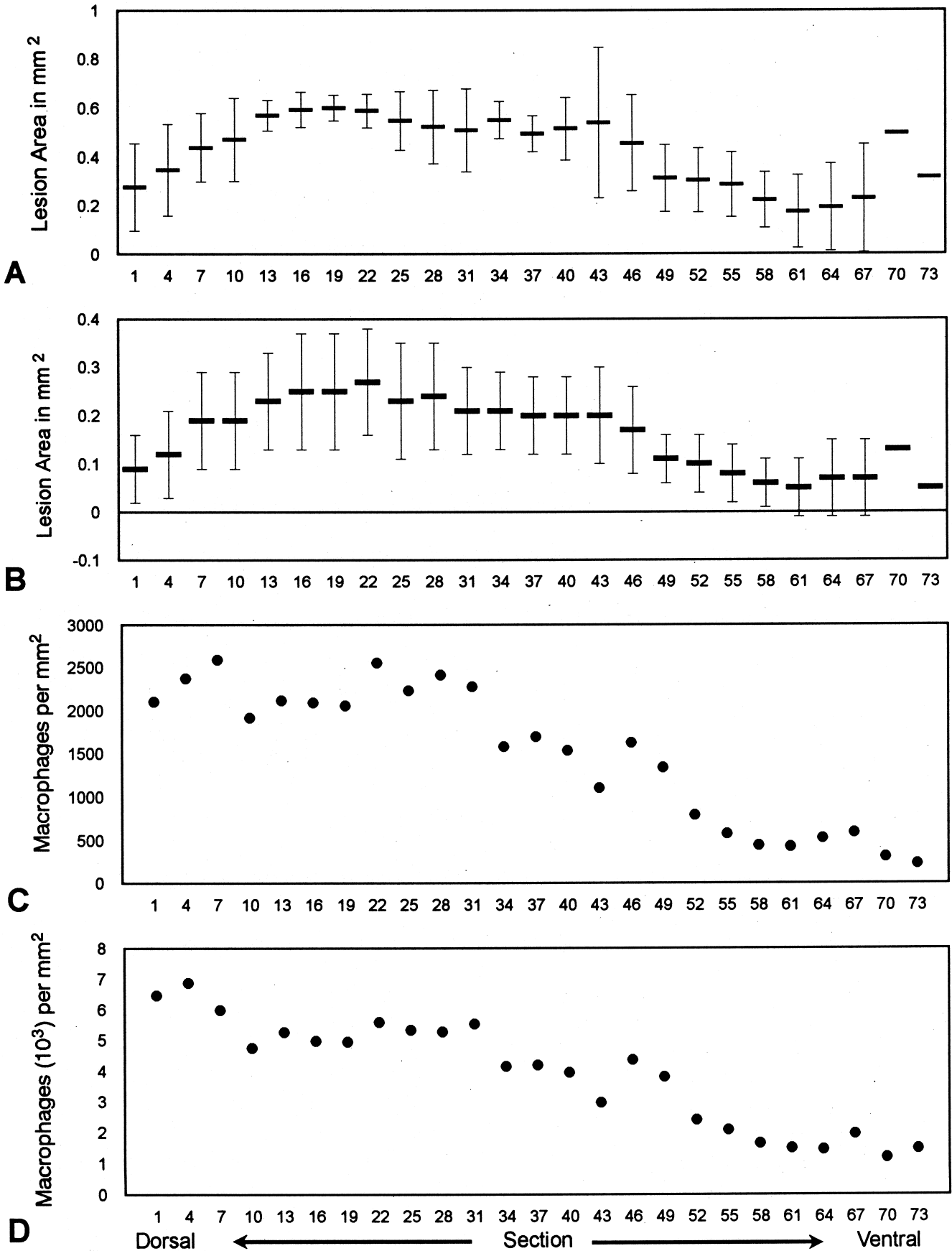


Fig. 8. Lesion area and macrophage density.

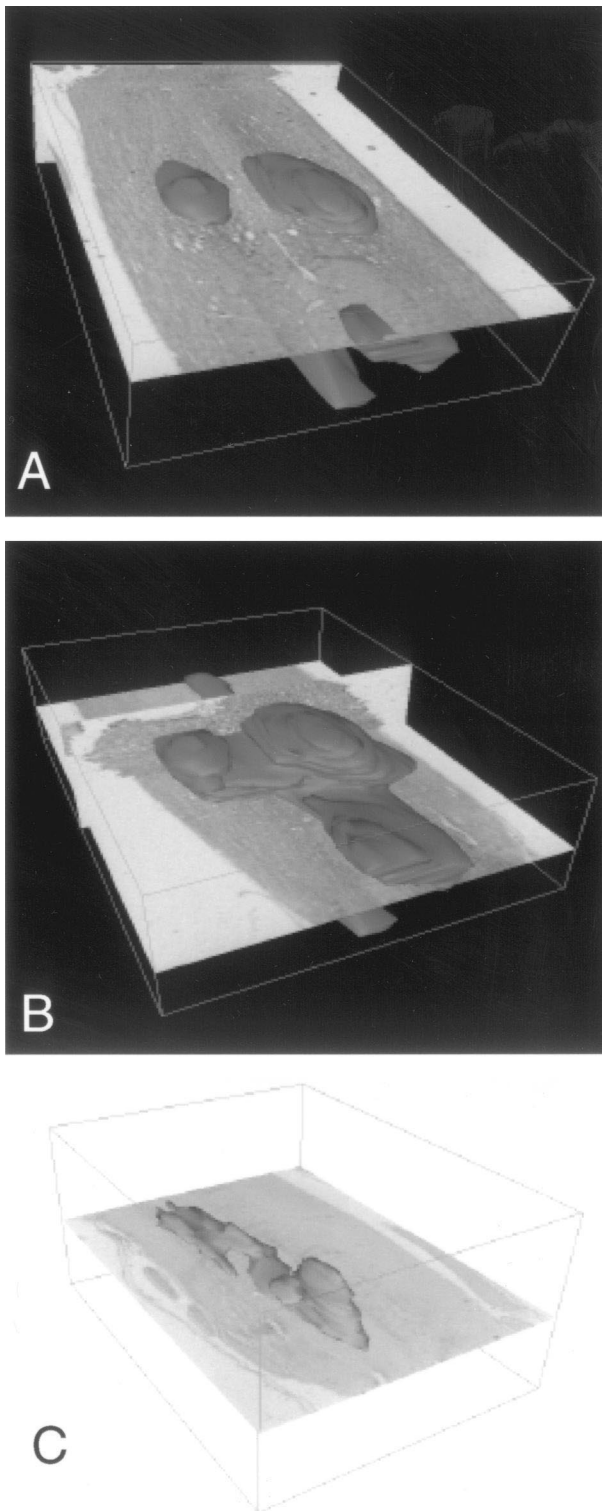


Fig. 9. Registration of surface reconstructions. (A) and (B) are 3-D surface reconstructions of the zone of injury superimposed within two orthogonal slices of the original data set. The lesion boundary was defined by ED1 labeled macrophages (refer to Section 2). The ventral surface of the cord is facing upward, rostral forward. Note the registration of the surface model within the histological section, and that the horizontal slice in B is more dorsal than in A. C is a similar image, reconstructed from another injured spinal cord injury, oriented caudal forward, ventral up.

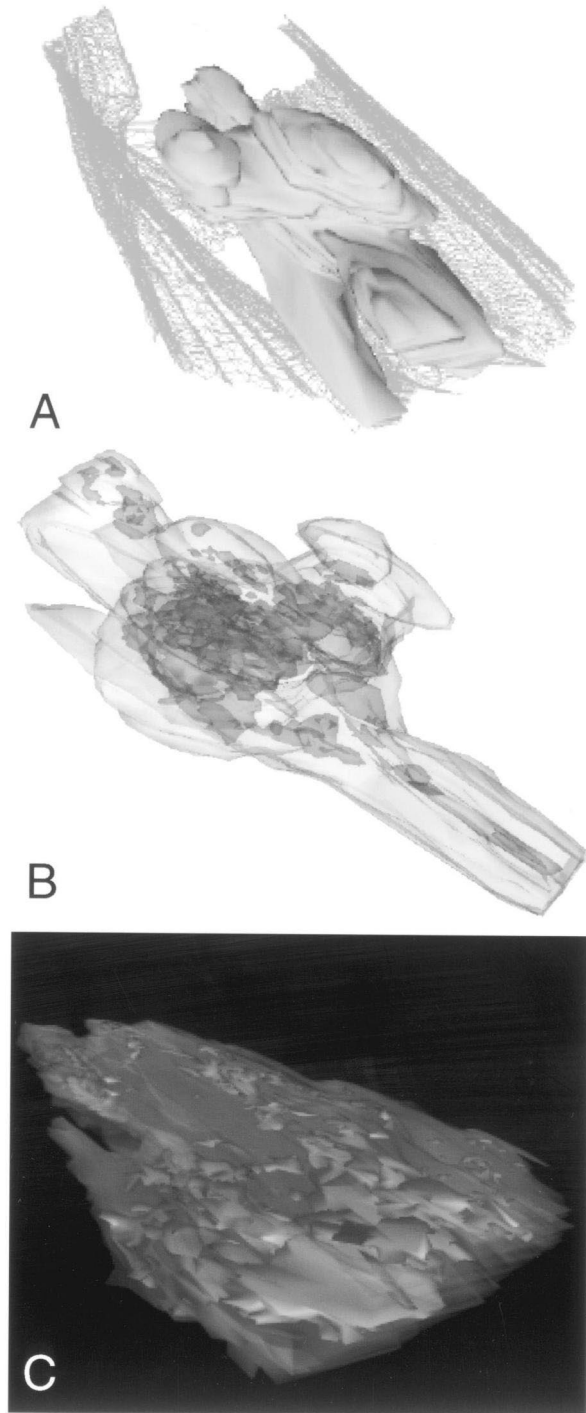


Fig. 10. Surface reconstruction of digitized images. (A) and (B) show surface reconstructions of the region of spinal cord injury defined by the boundary of labeled phagocytes. In A, the red wire frame model is the outside perimeter of the spinal cord segment containing the lesion. The most ventral sections have been removed, allowing an unobstructed view of the injury imbedded within it (rostral forward). In B, the same lesion as shown in A is visualized but, is made semi-transparent revealing the cystic structure (in red) within. The green mass within the large dorsal cyst is an island or raft of floating macrophages. This image has been rotated 180° along the long axis from that shown in A. In C, another reconstructed lesion containing cysts is shown by rendering the lesion surface semi-transparent. The lesion is oriented dorsal up and rostral forward.

3.8. Three-dimensional surface reconstruction: the subacute lesion as defined by phagocytes

Three-dimensional surface reconstructions involve management of the digitized image to emphasize boundaries and topology. Moreover, the algorithms we used to produce these reconstructions enable quantification of the region of interest (Bajaj et al., 1996a). Fig. 9A to C shows the solid surface rendering of the macrophagic lesion embedded within its histological section. Furthermore, these views reveal the correct registration of the lesion surface with the plane of the sections. In Fig. 10A a wire frame surface is used to reveal the injury zone within the spinal cord segment. The lesion can also be rendered semi-transparent to reveal this same anatomy, providing more details of the cysts at the expense of the lesion encompassing them (Fig. 10B and C). In Fig. 10B, the addition of a 'raft' or island of macrophages contained within a cyst is shown. Table 4 provides surface area and volumetric data derived from these two 3-D surface reconstructions.

These 3-D views show a lesion surface of complex shape. The surface area of the lesion in the two spinal cords shown are between 20–40% as large as the surface area of the entire segment of spinal cord containing it. The more severe injury occupies a volume approaching 18% of the cord segment, the less severe injury approximately 6%.

The more extensive regions of very small cysts could not be imaged at low power, and were not reconstructed.

4. Discussion

Even though several weeks have passed following a spinal cord injury, macrophage numbers are impressive, dominating the cellular makeup of the injury zone and defining the boundaries and overall shape of the subacute lesion. Their density within the unit area of the central lesion approaches the theoretical limit imposed on such isodiametric cells of approximately 12 μm diameter. Given this average diameter, about 8000 cells could be squeezed into a cross-sectional area of approximately 1 mm^2 . If we define the area of the lesion as that containing only compromised parenchyma inundated with phagocytes plus cystic regions (Fig. 8D; see also Blight, 1992), significant portions of the lesions in this study come very close to this upper limit. In the balance, up to 68% of this theoretical limit is occupied by macrophages.

Blight (1985) found little evidence for a substantial fall in the numbers of macrophages from between 7 days and over 3 months. This fact accounted for our choice of a sample time (3 weeks post-injury) where numbers of these cells would have peaked, and unlikely to have declined since the insult. This temporal peak also corresponds with that of hydrolytic enzymes found in the central lesion (reviewed by Blight, 1985). The large numbers of these

cells shown here supports Blight's hypothesis of macrophage mediated 'bystander damage' as an important contribution to 'secondary' injury — even if only based on their exclusion of other cell types at the injury site.

4.1. The method

To our knowledge, immunocytochemical identification of macrophage cells has not been coupled to a procedure aimed at rigorously determining their numbers, density, or to provide volumetric data in a CNS lesion. There are a number of markers for the macrophage, such as labels for the accumulation of acetylated low density lipoprotein (Pitas et al., 1981; Giulian et al., 1989). We have chosen the monoclonal antibody ED1 for a variety of reasons: (1) its commercial availability, aiding possible replicatory studies, (2) it is one of the most studied of this group, widely used, with a long history of use, and particularly reliable in technical preparation, (3) it predominantly recognizes mononuclear phagocytes of myelomonocytic lineage (as well as monocytes in blood and their precursors in marrow), (4) ED1 expression is associated with the activated state, or phagocytic status, of these scavenger cells (Damoiseaux et al., 1994), (5) it does not recognize several subtypes of macrophages (metalophilic spleen and subsinusoidal lymph node macrophages, resident macrophages of peripheral connective tissue) (Dijkstra et al., 1985; Polman et al., 1986; Damoiseaux et al., 1994). Particularly relevant for our purposes, ED1 does not recognize the inactivated resident microglia of the CNS. This monoclonal antibody identifies a glycolated protein, 90 000–110 000 MW, ubiquitously expressed in the cytosol (probably associated with phagolysosomal machinery) and weakly on the plasma membrane (Damoiseaux et al., 1994). Altogether, we believe ED1 to be the best choice for discrimination of immigrant mononuclear phagocytes invading the CNS injury and their resident scavenger colleagues, transformed amoeboid microglia, which may be indistinguishable from the activated macrophages (Giulian, 1987).

The methodology used here samples nearly all (ranging from 90 to 100%) of the lesion in any one histological section of the injured spinal cord. If we counted cells in every section, this would over represent cell number (since many cleaved cells would lie within the thickness of one section). Counting the macrophages within the lesion in every third 15 μm thick section (roughly the diameter of a single macrophage) estimates the number of these cells throughout the injury zone, while counting every 4th section would under-represent the actual numbers of these cells. Using profile counts of cells of a similar, or smaller, diameter to the section thickness could over represent the number due to object splitting (Coggeshall and Lekan, 1996), however, we have calibrated this by comparing computer assisted cell counts to actual counts made by a naive investigator. Furthermore, there was little actual

Table 4

Quantification of spinal cord segments, lesions, and cysts: comparative evaluation between 3-D surface reconstructions, geometric equations and 2-D morphometry

Rat no.	Three-dimensional morphometry ^a						Comparative data ^b			
	A	B	C	D	E	F	G	H	I	J
	Cord Volume (mm ³)	Cord Surface Area (mm ²)	Lesion Volume (mm ³)	Lesion Surface Area (mm ²)	Cyst Volume (mm ³)	Cyst Surface area (mm ²)	Cord Volume ^c (mm ³)	Cord Surface area ^d (mm ²)	Lesion Volume ^e (mm ³)	Lesion Volume ^f (mm ³)
Rat 1	9.2	46.3	1.7	20.2	0.2	9.2	9.4	30.1	1.1	4.3
Rat 7	14.3	62.5	0.9	13.0	0.1	6.9	17.0	38.3	0.9	1.1

^a The values in columns A to F are derived directly from 3-D surface reconstructions shown in Figs. 9 and 10.

^b The values in columns G to J are derived from the application of different methods of quantification.

^c Volumes (*V*) shown are derived from a modification of the elliptical area formula for spinal cord area used by Blight (1985), where $V = [(\pi ab) \times h]$ and *a* and *b* are one-half the major and minor axes of the ellipse (cord) and *h* is the length of the cord segment being measured. Column G values are not significantly different from those in column A ($P = 0.45$, paired Student's *t*, two-tailed).

^d Surface areas (*S*) shown are derived from the formula for an approximation of an elliptical cylinder, where $S = 2\pi \left[\frac{\sqrt{a^2 + b^2}}{2} \right] h + 2\pi ab$ and *a* and *b* are one-half the major and minor axes of the ellipse (cord) and *h* is the length of the cord segment being measured. Note: The values in column H are not significantly different from those in column B ($P = 0.12$, paired Student's *t*, two-tailed).

^e The volume of the lesions for each rat were derived from adding all surface area data obtained by 2-D morphometry for serial histological sections \times the section thickness. That data (column I) is not significantly different than the data in column C ($P = 0.5$, paired Student's *t*, two-tailed).

^f This volume (*V*) data is derived from a formula based on a frustum model of the spinal cord lesion, after Bresnahan et al. (1991), $V = 1/3h[B_1 + B_2 + (B_1 B_2)^{1/2}]$ where *B*₁ and *B*₂ are the areas of the cone bases, *h* is the distance between bases. The volumes in column J are not significantly different from the data shown in column C ($P = 0.45$, paired Student's *t*, two-tailed).

difference (and no statistical difference) between the visual counts of cells made by an investigator and by the computer. Comparisons between the volume and surface area data generated by different software (2-D and 3-D) provides additional support for the overall quantitative evaluation. For example, compilation of 2-D surface area data to provide volumes of two spinal lesions was not significantly different than that data derived by 3-D morphometry (Table 4).

To our knowledge, the last attempt at establishing the numbers of macrophages within the whole spinal cord lesion at several time periods post-injury was performed over a decade ago (Blight, 1985). This study employed (a) a visual identification of macrophages in semi-thin toluidine blue stained sections and (b) counting by a line sampling technique (Blight, 1983). Cell counts were made along 24 sample lines for each half cord. These estimates were expressed per unit area of the whole cord segment studied, and given as well for the outer 200 μ m circumferential rim of the lesion. These macrophage counts in the guinea pig are strikingly lower than those reported here for 3 weeks in the rat. Since the method used by Blight showed only a doubling (or less) in the peak numbers of macrophages between one week and 3 months, the differences between the two reports is probably not a function of the temporal dynamic of macrophage accumulation, rather, a difference produced by the method of counting cells or a species difference between rat and guinea pig (see Blight et al., 1997). This difference was unlikely to be due to injury severity since the lesions in his study were more severe than in ours, compromising the entire cord. There have been other attempts quantifying macrophage number within restricted sample region in the injured CNS (Giulian et

al., 1989; Giulian and Robertson, 1990). These counts have been used to compare the effect of treatments aimed at reducing macrophage numbers and not applied to determining the overall number or density of macrophages within the lesioned area.

4.2. Shape reconstruction of the subacute injury

Modern graphics hardware can quickly render an assembly of simple surface primitives, such as triangles or other polygons into 3-D images. Furthermore, the surface area and volume of a closed shape represented by a collection of primitives can be calculated. Our algorithms use polygons to represent the contours of a sliced object, and thereafter reconstruct 3-D shapes from such contours. These algorithms more accurately meet the computational demands of evaluating soft tissue injury than other commercial or public domain software.

It is commonplace to conceive of the mature injury to the spinal cord as something of a tube within a tube or a central core of necrosed parenchyma surrounded by a thin rim of sparing. This view is almost always seen in drawings of transverse sections through the injury zone, common to the older literature, and still prevalent in modern reports (Noble and Wrathall, 1985; Blight et al., 1991). Bresnahan et al. (1991) provided the first computer assisted three-dimensional reconstruction of the injury, defined by cresyl violet histology, and imaged by the amalgamation of transverse drawings made every 0.5 mm through the spinal segment of injury. The three-dimensional reconstruction and volumetric quantification algorithms applied here, both confirm and extend some aspects of this work. The actual shape of the subacute injury defined by

the boundaries between uninjured (macrophage free) and abnormal parenchyma is extremely complex with an extended surface area. We have applied the Bresnahan et al. (1991) formula for lesion volume to this subacute injury. This models the lesion as a frustum. Assuming that the early ischemic lesion (their data) is as complicated a shape as the macrophagic lesion (our data), their formula provides reasonable predictive power (Table 4). Volume and surface area data derived by modeling the cord as elliptical (after Blight, 1985) also appears useful (Table 4). Overall, the application of such simple models may be helpful in approximating such extremely complicated topologies, when more sophisticated computational power is either not available or demanded.

4.3. *The macrophage in CNS injury and reconstruction*

The macrophage is uniquely suited to mediate critical processes of healing, tissue reconstruction and regeneration. The cells are highly mobile and recruited to injury sites, as well as differentiating from circulating monocytes that are known to cross the blood brain barrier and other epithelial/endothelial ‘barriers’ by unknown mechanisms (Perry and Brown, 1992; Gordon, 1995). Macrophages are well known to be ‘professional scavengers’ playing a sometimes dominant role in the cytolysis and engulfment of dead and dying cells and their debris at the injury zone. This role also includes the removal of myelin debris in damaged nervous tissue, a job once assumed to be restricted to Schwann cells in peripheral nerves (Perry and Brown, 1992). The various intracellular products such as hydrolytic enzymes, and other moieties that contribute to this cellular clean up operation have been well discussed (Davies and Bonney, 1979; Gordon, 1995). This process of cellular debridement, especially the removal of myelin debris, appears important to the rate if not the success of peripheral nerve regeneration. Temporal differences in this phase of inflammation may lie at the basis of differences in outcome when comparing regeneration of the neural elements of the PNS and CNS (Perry and Brown, 1992).

Macrophages also mediate reconstructive phases of healing — not just the removal of cell debris following injury. The production of various cytokines such as interleukin 1 (IL-1), are known to regulate various aspects of immune and non-immune mediated processes and subsequently, the reconstruction phase following inflammation and healing (Stocum, 1995). Macrophages may also contribute to a ‘persuasive’ microenvironment in the CNS favoring axonal regeneration (David et al., 1990). In CNS tissue, macrophage synthesis of IL-1 and transforming growth factor beta (TGF β) together with activated amoeboid microglial scavengers is associated with increased neoangiogenesis and astroglial proliferation (Giulian, 1987). Astrocytes also synthesize these same compounds which together with macrophage cell specific products may oppose the activity of basic fibroblast growth

factor (bFGF) (which facilitates fibril scarring and endothelial proliferation). It is likely that reactive gliosis and hypervascularity in CNS lesions is not helpful to reconstruction and functional outcome following CNS injury (Reier et al., 1983; Reier and Houle, 1988; Blight, 1991). Recently Lazarov-Spiegler et al. (1996) suggest a biochemical suppression of the activated state of macrophages by the CNS. Perhaps the extraordinary numbers of macrophages in the subacute lesion reported here may be a function of a relatively poor phagocytic capability.

4.4. *The macrophage and cystic cavitation*

As expected, the dominating presence of macrophages is associated with cavitation of the spinal cord and Wallerian degeneration of white matter at distance from the focus of the injury. Regions of so-called ‘microcavitation’ (Kao and Chang, 1977) are characterized by extensive small holes in the parenchyma, each curiously the size of a single macrophage (these data). While some of these holes may be capillaries in cross-section (also on the order of 10 μ m in diameter) the large numbers and localization in white matter does not suggest a major component of ‘cavitated’ parenchyma to be due to the presence of vascular elements (see Blight, 1991). Perhaps such cavitation (particularly in white matter) may be formed by restricted phagocytosis of parenchyma by single cells. Interestingly however, the regions of severe cavitation within the spinal segment containing the lesion are not restricted to the dorsal part of the spinal cord — the site of peak macrophage numbers and the experimentally produced injury (Figs. 4 and 7). This supports the view that several mechanisms of cavity formation, including phagocytosis, act in concert to destroy parenchyma at the site of injury. However, the extensive inclusions of macrophages within forming cysts, even floating within these cysts as ‘rafts’ (these data and Blight, 1992) leaves no doubt that the activity of these cells leads to the cavitation and cyst formation within CNS soft tissue.

Acknowledgements

We appreciate the technical aid of Debra Bohnert and Aaron Harbath and the help with visualization and pictures by Daniel Schikore during the conduct of these experiments. Financial support was provided by Department of Defense — USAMRMC-DAMD17-94-J-4242 to R.B.B., AASERT DAAH04-93-G-101 to R.B.B., CDC/CIC grant #R49/CCR509137 to R.B.B., NSF grant CCR 92-22467 to R.B.B., AFSOR grants F49620-94-1-0080 to C.L.B., AASERT F69620-93-1-0553 to C.L.B., ONR grants N00014-96-1-0370 to C.L.B., AASDERT N00014-95-1-1025 to C.L.B. and support of the Center for Paralysis Research, and the Shastra Laboratory, Department of Computer Sciences, Purdue University, by the Canadian Spinal Research Organization. We thank Melyssa Haines

and Rosana Vargas for manuscript preparation and Dr John Turek and Dr Andrew Blight for their thoughtful suggestions on the text.

References

- Bajaj, C., Cole, E., Lin, K., 1996a. Arbitrary topology shape reconstruction from planar cross sections. *Graphical Models and Image Processing* 58, 524–543.
- Bajaj, C., Cole, E., Lin, K., 1996b. Boundary and 3-D triangular meshes from planar cross sections. *Proc. of the 5th International Imaging Roundtable*, Sandia National Labs, Report SAND 96-2301, VC-405, pp. 169–178.
- Blight, A.R., 1983. Cellular morphology of chronic spinal cord injury in the cat: analysis of myelinated axons by line sampling. *Neurosci.* 2, 521–543.
- Blight, A.R., 1984. Inflammatory responses following experimental spinal cord injury: A destructive effect of macrophages on axons and myelin? *Soc. Neurosci. Abs.* 10, 887.
- Blight, A.R., 1985. Delayed demyelination and macrophage invasion: A candidate for secondary cell damage in spinal cord injury. *Cent. Nerv. Sys. Trauma* 2, 299–315.
- Blight, A.R., 1991. Morphometric analysis of blood vessels in chronic experimental spinal cord injury: hypervascularity and recovery of function. *J. Neurolog. Sci.* 106, 158–174.
- Blight, A.R., Toombs, J.P., Bauer, M.S., Widmer, W.R., 1991. The effects of 4-Aminopyridine on neurological deficits in chronic cases of traumatic spinal cord injury in dogs: A phase I clinical trial. *J. Neurotrauma* 8, 103–119.
- Blight, A.R., 1992. Macrophages and inflammatory damage in spinal cord injury. *J. Neurotrauma* 9, s83–s91.
- Blight, A.R., 1993. Remyelination, Revascularization, and Recovery of Function in Experimental Spinal Cord Injury. In: Seil F.J. (Ed.). *Advances in Neurology: Neural Injury and Regeneration*, Vol. 59, pp. 91–103.
- Blight, A.R., Carwile Leroy, Jr., E., Heyes, M.P., 1997. Quinolinic acid accumulation in injured spinal cord: time course, distribution, and species differences between rat and guinea pig. *J. Neurotrauma* 14, 89–98.
- Bresnahan, J.C., Beattie, M.S., Stokes, B.T., Conway, K.M., 1991. Three-dimensional computer-assisted analysis of graded contusion lesions in the spinal cord of the rat. *J. Neurotrauma* 8, 91–97.
- Coggeshall, R.E., Lekan, H.A., 1996. Methods for determining numbers of cells and synapses: a case for more uniform standards of review. *J. Comp. Neurol.* 364, 6–15.
- Damoiseaux, J.G.M.C., Dopp, E.A., Calame, W., Choa, D., MacPherson, G.G., Dijkstra, C.D., 1994. Rat macrophage lysosomal membrane antigen recognized by monoclonal antibody ED1. *Immunology* 83, 140–147.
- David, S., Bouchard, O., Tsatas, O., Giftichristos, N., 1990. Macrophages can modify the non-permissive nature of the adult mammalian central nervous system. *Neuron* 5, 463–469.
- Davies, P., Bonney, R.J., 1979. Secretory products of mononuclear phagocytes: a brief review. *J. Reticuloendo. Soc.* 26, 37–47.
- Dijkstra, C.D., Dopp, E.A., Joling, P., Kraal, G., 1985. The heterogeneity of mononuclear phagocytes in lymphoid organs: distinct macrophage subpopulations in the rat recognized by monoclonal antibodies ED1, ED2 and ED3. *Immunology* 54, 589–599.
- Giulian, D., 1987. Ameboid microgila as effectors of inflammation in the central nervous system. *J. Neurosci. Res.* 18, 155–171.
- Giulian, D., Chen, J., Ingeman, J., George, J.K., Noponen, M., 1989. The role of mononuclear phagocytes in wound healing after traumatic injury to adult mammalian brain. *J. Neurosci.* 9, 4416–4429.
- Giulian, D., Robertson, C., 1990. Inhibition of mononuclear phagocytes reduces ischemic injury in the spinal cord. *Am. Neurolog. Assoc.* 27, 33–42.
- Gordon, S., 1995. The macrophage. *BioEssays* 17, 977–986.
- Kao, C.C., Chang, L.W., 1977. The mechanism of spinal cord cavitation following spinal cord transection. Part 1: a correlated histochemical study. *J. Neurosurg.* 46, 197–209.
- Lazarov-Spiegler, O., Solomon, A.S., Zeev-Brann, A.B., Hirschberg, D.L., Lavie, V., Schwartz, M., 1996. Transplantation of activated macrophages overcomes central nervous system regrowth failure. *FASEB J.* 10, 1296–1302.
- Noble, L., Wrathall, J., 1985. Spinal cord contusion in the rat: morphometric analyses of alterations in the spinal cord. *Exp. Neurol.* 88, 135–149.
- Perry, V.H., Brown, B.C., 1992. Role of macrophages in peripheral nerve degeneration and repair. *BioEssays* 14, 401–406.
- Perry, V.H., Andersson, P.B., Gordon, S., 1993. Macrophages and inflammation in the central nervous system. *TINS* 16, 268–273.
- Pitas, R.E., Innerarity, J.N., Weinstein, J.N., Mahley, R.W., 1981. Acetoacetylated lipoproteins used to distinguish fibroblasts from macrophages in vitro by fluorescence microscopy. *Arteriosclerosis* 1, 177–185.
- Polman, C.H., Dijkstra, C.D., Sminia, T., Koetsier, J., 1986. Immunohistological analysis of macrophages in the central nervous system of Lewis rats with acute experimental allergic encephalomyelitis. *J. Neuroimmunol.* 11, 215–222.
- Reier, P.J., Stensaas, L.J., Guth, L., 1983. The Astrocytic Scar as an Impediment to Regeneration in the Central Nervous System. In: Kao C.C., Bunge R.P., Reier R.J. (Eds.); *Spinal Cord Reconstruction*. CC Thomas, Springfield, IL, pp. 163–195.
- Reier, P.J., Houle, J.D., 1988. The glial scar: Its bearing on axonal elongation and transplantation approaches to CNS repair. In: Waxman, S.G. (Ed.), *Advances in Neurology*, Vol. 47: *Functional Recovery in Neurological Diseases*. Raven Press, New York, pp. 87–138.
- Stocum, D.L., 1995. *Wound Repair, Regeneration and Artificial Tissues*. Landes R.G. Company.
- Tator, C.H., Fehlings, M.G., 1991. Review of the secondary injury theory of acute spinal cord trauma with emphasis on vascular mechanisms. *J. Neurosurg.* 75, 15–26.
- Waibl, H., 1973. *Zur topographie der medulla spinalis der albinoratte (Rattus norvegicus)* Springer-Verlag, Berlin, New York.
- Young, W., Huang, P.P., Kume-Kick, J., 1995. Cellular, ionic, and biomolecular mechanisms of the injury process. In: Benzel, E.C., Tator, C.H., (Eds.), *Contemporary Management of Spinal Cord Injury*, AANS Publications Committee, pp. 27–42.